Paramagnetic Spin Seebeck Effect

Stephen M. Wu,* John E. Pearson, and Anand Bhattacharya
Materials Science Division, Argonne National Laboratory, Argonne, Illinois 60439, USA
(Received 9 February 2015; revised manuscript received 13 March 2015; published 5 May 2015)

We report the observation of the longitudinal spin Seebeck effect in paramagnetic insulators. By using a microscale on-chip local heater, we generate a large thermal gradient confined to the chip surface without a large increase in the total sample temperature. Using this technique at low temperatures (< 20 K), we resolve the paramagnetic spin Seebeck effect in the insulating paramagnets $Gd_3Ga_5O_{12}$ (gadolinium gallium garnet) and $DyScO_3$ (DSO), using either W or Pt as the spin detector layer. By taking advantage of the strong magnetocrystalline anisotropy of DSO, we eliminate contributions from the Nernst effect in W or Pt, which produces a phenomenologically similar signal.

DOI: 10.1103/PhysRevLett.114.186602 PACS numbers: 72.20.Pa, 72.25.-b, 75.76.+j

Thermal spintronics seeks to unite the world of heat transport with the world of magnetism, creating and detecting nonequilibrium spin transport phenomena for potential use in electronic and magnetic devices [1]. A phenomenon that has gathered a lot of recent attention is the spin Seebeck effect (SSE), where thermal gradients (∇T) in materials can generate spin currents ($\vec{J}_S$), which can subsequently be detected through the inverse spin Hall effect by using a normal metal with high spin orbit interaction (W and Pt) [2]. The SSE has been shown to exist in several insulating ferromagnets (FMs) in the longitudinal configuration ($\vec{J}_S \| \nabla T$) [3–8].

In this Letter, we show that, in addition to insulating ferromagnets, the longitudinal SSE can also be observed in insulating paramagnets (PMs). This is an unexpected result, because all models of the SSE involve nonequilibrium thermally excited spin waves, which paramagnetic materials nominally cannot support. Using micropatterned SSE devices with an on-chip heater, we examined two insulating paramagnetic materials: $Ga_3Ga_5O_{12}$ [gadolinium gallium garnet (GGG)] and $DyScO_3$ (DSO). GGG is a geometrically frustrated magnetic material and standard substrate material for thin films of the canonical insulating ferrimagnet $Y_3Fe_5O_{12}$ (YIG) [9–11]. DSO is another well-known substrate material typically used for the growth of epitaxial perovskite oxides [12].

A schematic of the device is presented in Fig. 1(a). A 5 nm layer of W or Pt is deposited into a 800 μm $\times$ 10 μm strip on a 7.5 mm $\times$ 7.5 mm $\times$ 0.5 mm GGG (111) or DSO (110) substrate, with a 100 nm MgO barrier for electrical isolation and a 50 nm Au heater layer. By sending a sinusoidal current to the heater at ω and lock-in detecting the resulting 2ω signal across the spin detector layer, we sensitively detect effects that are only due to Joule heating and the resulting thermal gradient [5,13]. With this method we generate a large thermal gradient at the surface of the chip localized near the heater wire, without substantially raising the temperature of the whole chip. This is due to the large power density applied across the 10 μm wide heater wire at relatively low total power [13].

The in-plane magnetic properties of our GGG (111) substrate were measured by using SQUID magnetometry [Fig. 1(b)]. The magnetization versus applied field data match the Brillouin function for an $S = 7/2$ paramagnet at high temperatures, but at low temperature there are deviations [14]. The deviations are presumably due to incipient order that is suppressed by frustration, leading to short-range magnetic order [16]. Despite an extrapolated Curie-Weiss temperature of -2.32 K from the M versus T data, there is no sign of long range order down to 2 K, which matches well with previous work on GGG.

A constant sinusoidal 1 V_{pp} signal was applied across the heater and a 60 Ohm load resistor at 3 Hz ($P_{\text{heater}} = 0.48$ mW$_{\text{rms}}$) in our device. The voltage across the spin detector layer was lock-in detected while the magnetic field was swept between ± 90 kOe. In all measurements the magnetoresistance of the heater layer contributes to only a $\sim 0.1\%$ change in heater power. The results are shown for GGG/W (5 nm) [Fig. 2(a)] and GGG/Pt [Fig. 2(b)] for different temperatures. These curves exhibit no hysteresis and qualitatively match the magnetization curves shown in Fig. 1(b). There are deviations in the

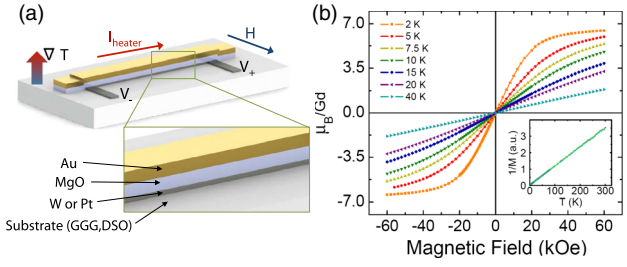

FIG. 1 (color online). (a) Schematic of a spin Seebeck device. (b) M versus H for GGG shown for various temperatures. The inset shows inverse magnetization versus temperature taken at 10 Oe.

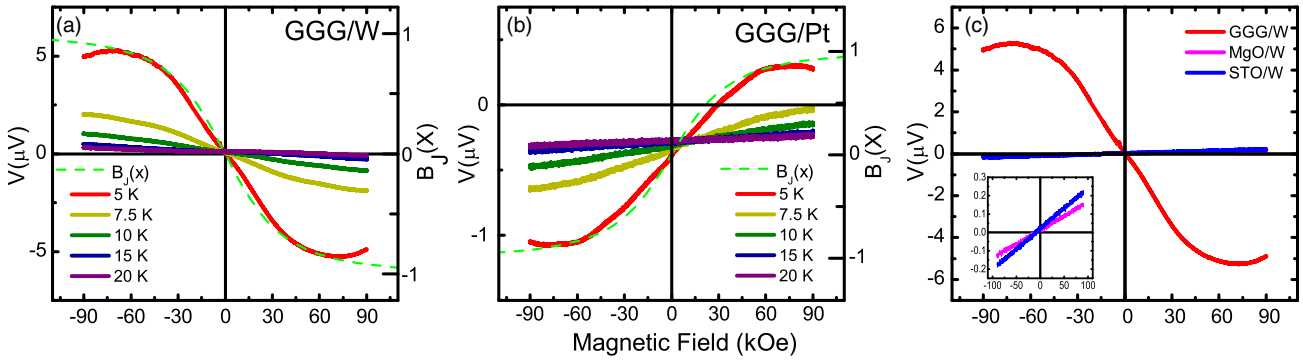

FIG. 2 (color online). Voltages generated by the SSE measured for various temperatures with both W (a) and Pt (b). The Brillouin function representing an $S = 7/2$ paramagnet at 5 K is overlaid. The magnetic field independent offsets are due to the conventional Seebeck effect. Control experiments with $SrTiO_3$ and MgO substrates are presented in (c) at 5 K along with data from (a). In all experiments, $P_{\text{heater}} = 0.48\ \text{mW}_{\text{rms}}$.

voltage trace from the ideal Brillouin function. This may be due to magnetic field dependence of the thermal conductivity in GGG or a Zeeman effect induced suppression also seen in SSE measurements in YIG [17]. The voltage responses for W and Pt are of opposite polarity, as would be expected if the effect was due to spin current since the spin Hall angles of W and Pt are opposite in sign. The shapes of the W and Pt curves, accounting for the sign change, are also very similar [14]. The magnitude of the response in W is much larger than that of Pt, since the resistivity of the deposited β-W phase is roughly 11 times larger. The measured voltage responses persist even when the measurement is performed with a dc excitation.

In Fig. 2(c), the voltage response from Fig. 2(a) at 5 K is compared to two devices fabricated on MgO and $SrTiO_3$ (STO) control substrates. MgO and STO both are nominally diamagnetic, with weak impurity-induced paramagnetism several orders of magnitude smaller than in GGG [18]. In both control devices we see a weak response with the *opposite* sign, an order of magnitude smaller than the GGG/W sample. The measured response is presumably from the Nernst effect of the underlying W. These data suggest that the effect from Figs. 2(a) and 2(b) comes from the paramagnetic SSE in GGG. Separate measurement on a GGG/Cu(2 nm)/Pt(5 nm) device results in the same behavior as in the GGG/Pt device [14]. This is evidence that proximity magnetism at the GGG/W and GGG/Pt interface is not the origin of the observed signal. More information on control experiments is included in Supplemental Material [14].

The voltage response $[V(H = 35\,\text{kOe}) - V(H = -35\,\text{kOe})]$ with respect to temperature is presented in Fig. 3 for GGG/W and STO/W devices. The heater power varies with temperature from 0.51 mW_{rms} at 300 K to 0.48 mW_{rms} at 5 K, due to variations in the heater resistance. The voltage response for the STO/W device is positive throughout and flattens out at low temperature, while the voltage response of the GGG/W device is negative and grows quickly with decreasing temperature. These observations indicate that the effect originates within GGG and not from W.

For the PM SSE there is a T^{-1} dependence due to the Curie-Weiss law ($\chi = C/T - \Theta_{\text{CW}}$), and for the Nernst effect there is a T dependence from the Mott relation $[\alpha_{xy} = (\pi^2 k_b^2 T/3e)(\partial\sigma_{xy}/\partial E)_{E_F}]$. Here, C is the Curie constant, Θ_{CW} is the Curie-Weiss temperature, α_{xy} is the transverse Nernst conductivity, and σ_{xy} is the transverse electrical conductivity. By using an on-chip heater at nearly constant power, the thermal gradient will be proportional to the thermal conductivity of the heated material [13]. This is because the back side of the chip is solidly heat sinked to the cryostat, and we are effectively sending a constant heat current through the stack (analogous to a current-biased voltage measurement). Here, the temperature-dependent measurements will inherently contain the temperature

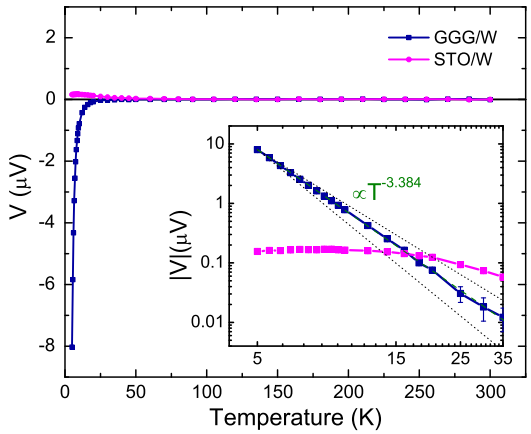

FIG. 3 (color online). The magnitude of the voltage response, as defined as the difference in voltages at ±35 kOe, for GGG and STO with respect to temperature. Data were taken at ±35 kOe to remain in the linear regime of M versus H. The inset represents the same data on a log-log scale, with the two dotted lines representing a T^{-4} and T^{-3} dependence.

dependence of thermal conductivity of the material, where lower thermal conductivity leads to larger ∇T. From kinetic theory, GGG thermal conductivity at low temperatures behaves close to T^3 due to its relation to phonon heat capacity [19,20]. On the other hand, for W at low temperatures the thermal conductivity behaves as T due to its relation to electronic heat capacity [21,22]. An additional factor at low temperatures is the thermal Kapitza resistance at the metal-insulator interface, since it will generate a discontinuous jump in temperature between W and either GGG or STO. SSE models exist for spin current generation from both a bulk thermal gradient [23] and an interfacial temperature difference between the spin source and spin detector [24]. Since at low temperatures the Kapitza conductance also scales as T^3, it is not possible to differentiate this effect from that of the temperature dependence of the thermal conductivity of GGG [25]. Regardless, since the Kapitza resistance matters only for the SSE, accounting for all temperature-dependent factors, a Nernst signal would be temperature independent, and a PM SSE signal would have a T^{-4} dependence:

$$V_{\mathrm{SSE}} \propto \frac{C}{T}\left(\frac{1}{\kappa_{\mathrm{ph}}}+\frac{1}{\kappa_{\mathrm{int}}}\right) \propto \frac{C}{T}\left(\frac{1}{T^3}+\frac{1}{T^3}\right) \propto \frac{1}{T^4}, \qquad (1)$$

$$V_N \propto \frac{\pi^2 k_b^2 T}{3e}\left(\frac{\partial \sigma_{xy}}{\partial E}\right)_{E_F}\left(\frac{1}{\kappa_{\mathrm{el}}}\right) \propto (T)\left(\frac{1}{T}\right) \propto 1. \qquad (2)$$

We see that the GGG/W device varies as $T^{-3.384}$, while the STO/W device is nearly constant. This suggests that the effect in GGG/W is due to the PM SSE from GGG, while in the STO/W device it is consistent with the Nernst effect. The deviation from the ideal T^{-4} behavior in GGG/W may be due the temperature dependence of the SSE, which has been shown in many experiments to decrease with temperature due to a decrease in thermal magnon population [23,26], deviations from ideal T^{-3} behavior of the Kapitza resistance [27], or the low temperature behavior of the spin mixing conductance at the interface [28].

To fully eliminate the possibility of the Nernst effect, a W (5 nm) device was created on a paramagnetic DSO (110) substrate. Since DSO has strong magnetocrystalline anisotropy [12], an applied magnetic field may generate a magnetization that is noncollinear to the field, allowing us to separate the Nernst effect and the SSE. Figure 4(a) shows the favored magnetization plane for the DSO (110) substrate used. Since the SSE is sensitive only to in-plane magnetization, the effect will be different for fields along the magnetic easy axis in the [−110] direction and the hard axis in the [001] direction oriented along the chip edges. Figure 4(b) shows that the magnetization along the [001] direction is ∼49 times smaller than in the [−110] direction at 3 K with the same applied magnetic field of 100 Oe. These data also show that DSO goes through a magnetic phase transition from the high temperature paramagnetic phase to an antiferromagnetic phase at 3.1 K. Angular-dependent voltage versus magnetic field measurements were made with several different SSE device orientations shown in Fig. 4(c). In an isotropic system, each device should have a phase-shifted $\cos(\phi+\phi_0)$ dependence. The phase shift ϕ_0 arises from the orientation of the device axis relative to the applied magnetic field. With additional anisotropy, devices will show nonsinusoidal behavior as seen in Fig. 4(c). Since device 2 is parallel to the easy axis, and no magnetization can develop with a component perpendicular to the device axis, the resulting response is a purely sinusoidal signal, presumably arising from the Nernst effect in W. Figure 4(d) shows the remainder of each voltage response after a modeled Nernst signal has been

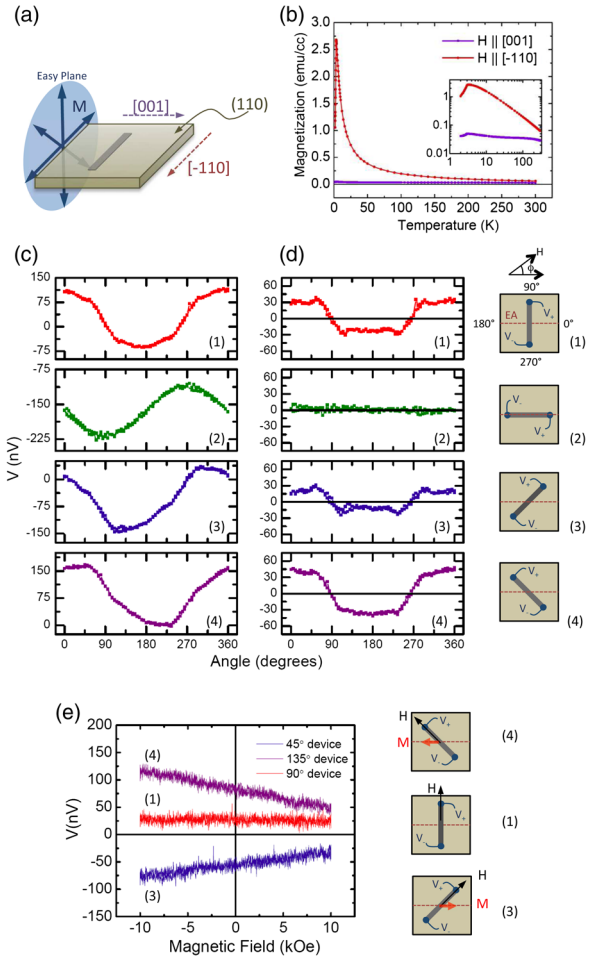

FIG. 4 (color online). (a) A schematic of the magnetic anisotropy for a $DyScO_3$ (110) substrate. (b) Temperature-dependent magnetization at 100 Oe. (c) Angular-dependent voltage responses with a constant 10 kOe applied field and a constant 1.87 mW_{rms} applied power at 5 K. The second column (d) represents the remainder of the response after a modeled Nernst signal has been subtracted. The geometry of each device is schematically shown to the right. (e) Voltage versus magnetic field with the same 1.87 mW_{rms} at 5 K, with a magnetic field applied along the axis of the device.

subtracted. The magnitude of the modeled Nernst signal was selected by using the ansatz that the remaining signal must be symmetric about the 180° axis due to the symmetry of the magnetic anisotropy of DSO. These magnitudes match well with the expected size of the Nernst effect based on measurements from STO/W devices. Each device except for device 2 has a PM SSE component left over with the *same* ϕ dependence corresponding to the easy axis of the chip and *not* the device orientation, consistent with our initial assumption. The ϕ dependence of this remaining signal is nonsinusoidal and is possibly due to an out-of-plane component of magnetization [12] or a consequence of the SSE in systems with large anisotropy.

By orienting the magnetic field along the axis of the device, we can eliminate the Nernst effect, since this occurs only for a magnetic field perpendicular to the device axis. In Fig. 4(e), the voltage response for three devices with magnetic fields applied along the device axes are shown. Both devices at 45° angles to the easy axis show a measurable voltage, while the device perpendicular to the easy axis does not. This would not be the case unless the PM SSE caused a measurable spin current due to a magnetization that is noncollinear to the applied field. The magnitude of the SSE in DSO is smaller than in GGG, due to the low thermal conductivity of DSO causing the chip surface to be at a much higher temperature for similar applied heater powers [14]. Since the magnitude of the SSE in these systems decreases sharply with increasing temperature, this strongly reduces the measured signal. The voltage responses in all experiments with DSO/W have an opposite polarity to those in GGG/W, indicating that DSO has a negative spin Seebeck coefficient which has also recently been seen in some compensated ferrimagnetic systems [29,30].

Currently, there are several theories surrounding the SSE, but, since all theories involve magnetic materials, each is based on magnons interacting with phonons and electrons. The longitudinal SSE on insulating ferromagnets was first discussed as an imbalance between thermal spin pumping from the FMs to the normal metal and spin current backflow caused by thermal noise from the normal metal to the FMs [24,31,32]. More recent models have focused on a bulk spin current caused by the nonequilibrium generation of thermal magnons within the FMs [23,33]. Here, a higher population of magnons is generated in higher temperature regions and a spin current is generated due to magnon diffusion.

To reconcile the existence of the SSE in paramagnetic materials with current theory, magnons must be allowed to exist. In paramagnets without magnetic interactions, propagating spin waves are not allowed. However, paramagnetic states in ferromagnets above T_C and antiferromagnets above T_N have been shown to support dispersive spin fluctuations similar to spin waves [34–37]. These "sloppy spin waves" or paramagnons can exist up to several times T_C and T_N, implying short range magnetic interactions still allow for damped short wavelength magnetic excitations without the existence of long range magnetic order [38–40]. Similarly, in systems where geometric frustration suppresses long range magnetic order, short range interactions can also cause spin-wave-like excitations to form [41]. Both GGG and DSO fit well within these models, since DSO is a conventional antiferromagnet (AFM) that undergoes a transition at 3.1 K and GGG is a geometrically frustrated AFM. GGG has no long range magnetic order down to $T \ll \Theta_{CW}$ [9] but shows signs of short range correlations up to at least 5 K, both through neutron scattering studies [10] as well as in our own magnetization measurements [14]. This connection was also made in recently published work on spin pumping in the PM phase of La_2NiMnO_6 above its T_C, where it is suggested that short range magnetic order allows for the generation of spin current when the electron paramagnetic resonance condition is met [42]. In La_2NiMnO_6 the role of itinerant electrons is important, because a measurable conductivity exists in the PM phase, but for DSO and GGG the only potential source of spin current is through magnon transport, because both are strongly insulating at all temperatures.

We have shown that a measurable spin current can be generated in paramagnetic GGG and DSO due to the SSE. This represents a demonstration of the SSE without ferromagnetic materials. The magnitude of the measured voltage response at low temperatures is comparable in magnitude to those measured in YIG/Pt and YIG/W devices at room temperature. Since all models of the SSE involve magnon transport, either the paramagnetic phases of GGG and DSO can sustain spin excitations or existing SSE models must be revised to include a new mechanism that would allow for spin current generation in a paramagnetic insulator. Further work on correlating a measurable SSE signal to measurable spin wave dynamics in paramagnetic materials is necessary to clarify the role of short range magnetic interactions for the paramagnetic SSE.

All authors acknowledge support of the U.S. Department of Energy (DOE), Office of Science, Basic Energy Sciences (BES), Materials Sciences and Engineering Division. The use of facilities at the Center for Nanoscale Materials was supported by the U.S. DOE, BES under Contract No. DE-AC02-06CH11357.

*swu@anl.gov

[1] G. E. W. Bauer, E. Saitoh, and B. J. van Wees, Nat. Mater. **11**, 391 (2012).
[2] C.-F. Pai, L. Liu, Y. Li, H. Tseng, D. Ralph, and R. Buhrman, Appl. Phys. Lett. **101**, 122404 (2012).
[3] K. Uchida, H. Adachi, T. Ota, H. Nakayama, S. Maekawa, and E. Saitoh, Appl. Phys. Lett. **97**, 172505 (2010).
[4] K.-i. Uchida, T. Nonaka, T. Ota, and E. Saitoh, Appl. Phys. Lett. **97**, 262504 (2010).

[5] S. M. Wu, J. Hoffman, J. E. Pearson, and A. Bhattacharya, Appl. Phys. Lett. **105**, 092409 (2014).
[6] R. Ramos *et al.*, Appl. Phys. Lett. **102**, 072413 (2013).
[7] D. Meier, T. Kuschel, L. Shen, A. Gupta, T. Kikkawa, K.-i. Uchida, E. Saitoh, J.-M. Schmalhorst, and G. Reiss, Phys. Rev. B **87**, 054421 (2013).
[8] K. Uchida, T. Nonaka, T. Kikkawa, Y. Kajiwara, and E. Saitoh, Phys. Rev. B **87**, 104412 (2013).
[9] P. Schiffer, A. P. Ramirez, D. A. Huse, and A. J. Valentino, Phys. Rev. Lett. **73**, 2500 (1994).
[10] O. A. Petrenko, C. Ritter, M. Yethiraj, and D. M. Paul, Phys. Rev. Lett. **80**, 4570 (1998).
[11] P. P. Deen, O. Florea, E. Lhotel, and H. Jacobsen, Phys. Rev. B **91**, 014419 (2015).
[12] X. Ke, C. Adamo, D. G. Schlom, M. Bernhagen, R. Uecker, and P. Schiffer, Appl. Phys. Lett. **94**, 152503 (2009).
[13] S. M. Wu, F. Y. Fradin, J. Hoffman, A. Hoffmann, and A. Bhattacharya, J. Appl. Phys. **117**, 17C509 (2015).
[14] See Supplemental Material at http://link.aps.org/supplemental/10.1103/PhysRevLett.114.186602 for additional control experiments, which includes Refs. [13,15,19].
[15] A. Aqeel, I. J. Vera-Marun, B. J. van Wees, and T. Palstra, J. Appl. Phys. **116**, 153705 (2014).
[16] P. Schiffer, A. P. Ramirez, D. A. Huse, P. L. Gammel, U. Yaron, D. J. Bishop, and A. J. Valentino, Phys. Rev. Lett. **74**, 2379 (1995).
[17] K. Uchida, M. Ishida, T. Kikkawa, A. Kirihara, T. Murakami, and E. Saitoh, J. Phys. Condens. Matter **26**, 343202 (2014).
[18] M. Khalid, A. Setzer, M. Ziese, P. Esquinazi, D. Spemann, A. Pöppl, and E. Goering, Phys. Rev. B **81**, 214414 (2010).
[19] Y. Hakuraku, Jpn. J. Appl. Phys. **22**, 1465 (1983).
[20] B. Daudin, R. Lagnier, and B. Salce, J. Magn. Magn. Mater. **27**, 315 (1982).
[21] C. Kittel, *Introduction to Solid State Physics* (Wiley, New York, 1976), Vol. 8.
[22] K. Mendelssohn and H. Rosenberg, Proc. Phys. Soc. London Sect. A **65**, 388 (1952).
[23] S. M. Rezende, R. L. Rodríguez-Suárez, R. O. Cunha, A. Rodrigues, F. L. A. Machado, G. A. F. Guerra, J. C. L. Ortiz, and A. Azevedo, Phys. Rev. B **89**, 014416 (2014).
[24] H. Adachi, J.-i. Ohe, S. Takahashi, and S. Maekawa, Phys. Rev. B **83**, 094410 (2011).
[25] A. Kent, *Experimental Low Temperature Physics* (Springer Science, New York, 1993).
[26] K. Uchida, T. Ota, H. Adachi, J. Xiao, T. Nonaka, Y. Kajiwara, G. Bauer, S. Maekawa, and E. Saitoh, J. Appl. Phys. **111**, 103903 (2012).
[27] E. T. Swartz and R. O. Pohl, Rev. Mod. Phys. **61**, 605 (1989).
[28] M. Weiler *et al.*, Phys. Rev. Lett. **111**, 176601 (2013).
[29] Y. Ohnuma, H. Adachi, E. Saitoh, and S. Maekawa, Phys. Rev. B **87**, 014423 (2013).
[30] S. Geprägs *et al.*, arXiv:1405.4971.
[31] J. Xiao, G. E. Bauer, K.-c. Uchida, E. Saitoh, and S. Maekawa, Phys. Rev. B **81**, 214418 (2010).
[32] H. Adachi, K.-i. Uchida, E. Saitoh, and S. Maekawa, Rep. Prog. Phys. **76**, 036501 (2013).
[33] U. Ritzmann, D. Hinzke, and U. Nowak, Phys. Rev. B **89**, 024409 (2014).
[34] P. A. Fleury, Phys. Rev. **180**, 591 (1969).
[35] M. F. Collins and B. D. Gaulin, J. Appl. Phys. **55**, 1869 (1984).
[36] Y. Ishikawa, Y. Noda, Y. J. Uemura, C. F. Majkrzak, and G. Shirane, Phys. Rev. B **31**, 5884 (1985).
[37] R. Doubble, S. M. Hayden, P. Dai, H. A. Mook, J. R. Thompson, and C. D. Frost, Phys. Rev. Lett. **105**, 027207 (2010).
[38] J. A. Hertz and M. A. Klenin, Physica (Amsterdam) B+C **91**, 49 (1977).
[39] T. Moriya, J. Phys. Soc. Jpn. **51**, 420 (1982).
[40] K. Tomita and T. Kawasaki, Prog. Theor. Phys. **45**, 1 (1971).
[41] F. Mila, D. Poilblanc, and C. Bruder, Phys. Rev. B **43**, 7891 (1991).
[42] Y. Shiomi and E. Saitoh, Phys. Rev. Lett. **113**, 266602 (2014).